The longitudinal and transverse magnetoresistivities and the AC susceptibility of $Fe_{10}Pt_{90}$

1994 J. Phys.: Condens. Matter 6 3045

(http://iopscience.iop.org/0953-8984/6/16/010)

J. Phys.: Condens. Matter 6 (1994) 3045–3057. Printed in the UK

The longitudinal and transverse magnetoresistivities and the AC susceptibility of $Fe_{10}Pt_{90}$

P A Stampe, X Chen†, Z Wang‡, H P Kunkel and Gwyn Williams
Department of Physics, University of Manitoba, Winnipeg, Canada R3T 2N2

Received 18 August 1993, in final form 16 December 1993

Abstract. A summary of detailed measurements of field and temperature dependent magnetic and transport properties in $Fe_{10}Pt_{90}$ is presented, with particular emphasis on attempting to evaluate the influence of spin–orbit coupling. Analysis of the field dependent AC susceptibility near the Curie temperature $T_C \simeq 170$ K enables effective exponent values to be estimated, although the presence of magnetic anisotropy arising from spin–orbit coupling prevents asymptotic exponent values from being found. The anisotropy of the magnetoresistance in this system also originates from spin–orbit coupling, and this behaviour is discussed in terms of both itinerant and localized models. A number of estimates for T_C are deduced from these different measurements and compared.

1. Introduction

Considerable recent interest has been generated by the observation of giant magnetoresistance (GMR) in both magnetic multilayer systems [1–4] and granular alloys [5–7]. For the latter, much current effort has been directed towards investigating links between fabrication conditions and the overall magnitude of the GMR, and a number of interesting correlations has been established [8]. One interesting, though negative, result that has also been reported concerns (possibly) *granular* FePt, which does *not* exhibit GMR, with attendant speculation [9] regarding the role played by spin–orbit coupling (in Pt) in this phenomenon. Consequently, we have undertaken a detailed study of crystalline $Fe_{10}Pt_{90}$; the composition chosen is close to that at which giant anomalies occur in granular systems, while at current levels of understanding the crystalline environment provides fewer complications against which such effects might be assessed.

Reported below is a summary of detailed measurements of the longitudinal and transverse magnetoresistivities ($\rho_\parallel$ and $\rho_\perp$ respectively) of $Fe_{10}Pt_{90}$ at 4.2 K in applied fields ($\mu_0 H_a$) up to 1 T (beyond which the magnetoresistance is saturated), of the zero-field resistivity $\rho(0, T)$ and its temperature derivative $d\rho/dT$ for temperatures $150 < T < 180$ K, of the low-field resistive anisotropy (LFRA) ($\rho_\parallel - \rho_\perp$) in applied fields of 2.5, 6, 10 and 13 mT for $150 < T < 180$ K, of the field dependent AC susceptibility $\chi_{AC}(H_a, T)$ ($0 \leqslant \mu_0 H_a \leqslant 0.1$ T; $150 < T < 200$ K) in the vicinity of the Curie temperature $T_C (\simeq 173$ K) and of the coercive field $\mu_0 H_c$ (from 'butterfly loops', namely $\chi_{AC}(H_a, T)$ versus H_a) for various fixed temperatures $T \leqslant T_C$. The LFRA measurements are also

† Present address: Centre for the Physics of Materials, Ernest Rutherford Physics Laboratory, McGill University, Montreal, Canada H3A 2T8.

‡ Currently at Department of Physics, Dalhousie University, Halifax, Nova Scotia, Canada B3H 3J5.

0953-8984/94/163045+13$19.50

discussed in terms of itinerant and localized model approaches, and a detailed calculation for this parameter is presented based on the latter approach [10].

While the magnetoresistance itself is dominated by spin dependent effects, the *anisotropy* $(\rho_{\parallel} - \rho_{\perp})$ reflects the influence of spin–orbit coupling [11].

2. Experimental details

A sample of nominal composition $Fe_{10}Pt_{90}$ was prepared by arc melting from starting materials of 4N purity. Following repeated inversion and remelting (with negligibly small melting losses) the alloy was cold rolled (between protective plastic sheets) into a foil of thickness $\sim 10^{-4}$ m. This foil was etched, washed and then annealed at 950 °C for 72 h at 10^{-6} Torr, after which it was water quenched. While the high solubility of Fe in Pt should ensure that samples fast cooled from the melt are metallurgically homogeneous, this annealing and quenching procedure was adopted following the comments of Ododo [12] regarding its influence on the sharpness of the magnetic transition. Samples suitable for transport ($(0.1 \times 2 \times 35)$ mm^3) and susceptibility ($(0.1 \times 2 \times 17)$ mm^3) measurements were then made.

AC susceptibility measurements were carried out at 2.4 kHz in a phase locked susceptometer [13] with a driving field of 3.5 μT and various collinear static biasing fields (applied along the largest sample dimension). Details of the temperature measurement and of various corrections have been given previously [14].

The resistivity sample was mounted on a high-thermal-conductivity Cu block, which was inserted into a wide-bored (5 cm) superconducting solenoid; this block could be rotated through 90° about an axis perpendicular to that of the solenoid, thus enabling the longitudinal and transverse magnetoresistance to be measured at the same temperature; temperatures were stabilized and measured using a carbon-glass thermometer in conjunction with a Lake Shore model 520 controller. The differential resistivity ratio $[\rho(H_a, T) - \rho(0, T)]/\rho(0, T)$ was measured with a precision of a few ppm using a low-frequency (37 Hz), four-probe AC method [15], with currents of typically 60 mA applied along the largest sample dimension. The temperature derivative, $d\rho/dT$, was estimated from similar measurements of the ratio $[\rho(0, T + \Delta T) - \rho(0, T)]/\rho(0, T)$ for temperature increments $\Delta T \sim 1$ K throughout the region of interest. Finally, absolute resistivities were found from measurements of $\rho(0, 110\ \text{K})$, the latter being subject to an error of about $\pm 1\%$ arising principally from shape factor uncertainties.

3. Results and discussion

3.1. AC susceptibility

Figure 1 shows a selection of AC susceptibility ($\chi_{ac}(H_a, T)$) data (corrected for background and demagnetizing effects [14]) for applied fields in the range $0 \leqslant \mu_0 H_a < 1.5 \times 10^{-2}$ T in the vicinity of the Curie temperature T_C. Analysis of these data (summarized in figures 2–4) is based on the usual static scaling law [16], namely

$$\chi(h, t) = t^{-\gamma} F(h/t^{\gamma+\beta}) \tag{1}$$

where $h \sim H_i/T_C$ and $t = |T - T_C|/T_C$ are the conventional linear scaling fields. Equation (1) leads to the following power-law relationships between

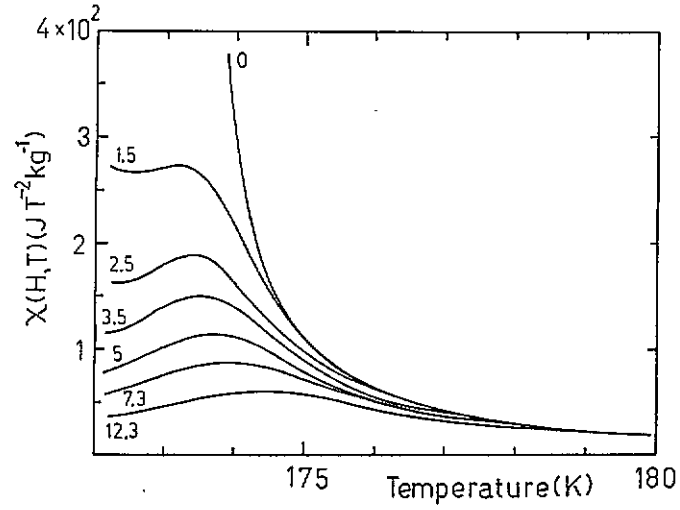

Figure 1. The true susceptibility $\chi(H, T)$ (in J T^{-2} kg^{-1}) (corrected for background and demagnetizing effects) plotted against temperature (in K) in the vicinity of the Curie temperature. The number marked against each curve is the estimated static biasing field $\mu_0 H_i$ (in mT).

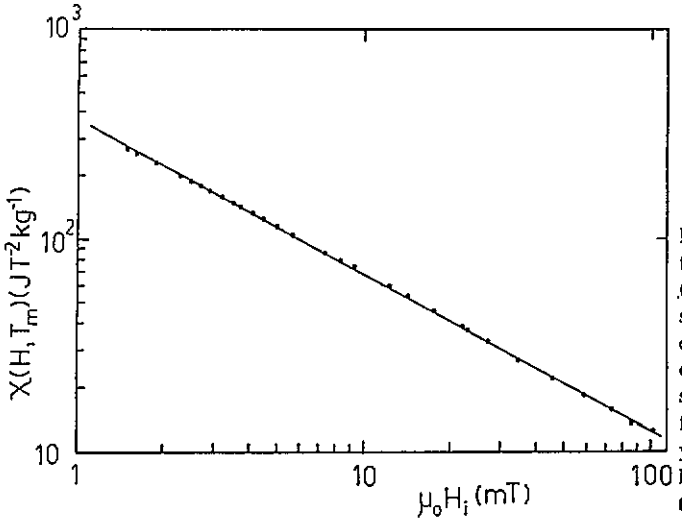

Figure 2. The critical peak susceptibility $\chi(H, T_m)$ (in J T^{-2} kg^{-1}) (taken from data similar to those shown in figure 1) plotted against the estimated internal field $\mu_0 H_i$ (in mT) on a double logarithmic scale. The solid line represents a least-squares fit of equation (3) to the data and yields the δ-value quoted in the text. Errors are comparable to or smaller than the point size.

(i) the zero-field susceptibility and the (reduced) temperature:

$$\chi(0, t) \propto t^{-\gamma} \qquad T > T_C \tag{2}$$

(ii) the peak amplitude $\chi(h, t_m)$ of the field dependent susceptibility (evident in figure 1) and field h:

$$\chi(h, t_m) \propto h^{1/\delta - 1} \tag{3}$$

and

(iii) the peak temperature $t_m (= (T_m - T_C)/T_C)$ of the field dependent susceptibility and field h:

$$t_m \propto h^{(\gamma+\beta)^{-1}}. \tag{4}$$

A detailed discussion of the procedure followed to implement a systematic, self-consistent fit of (2)–(4) to these data has been given previously [14] and will not therefore be repeated here; a summary of such fits is outlined below.

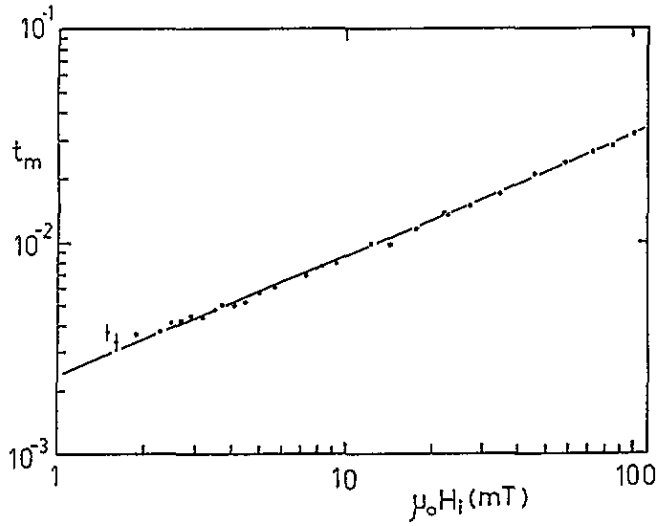

Figure 3. The (reduced) peak temperature t_m (also taken from data similar to those shown in figure 1) plotted against the estimated internal field $\mu_0 H_i$ (in mT) on a double logarithmic scale. The line drawn corresponds to a least-squares fit of equation (4) to these data and yields the value for $(\gamma + \beta)$ quoted in the text. The error bars shown represent an uncertainty of 50 mK in the temperature difference $(T_m - T_C)$ (T_C has been taken as 172.75 K) and are only important at low fields.

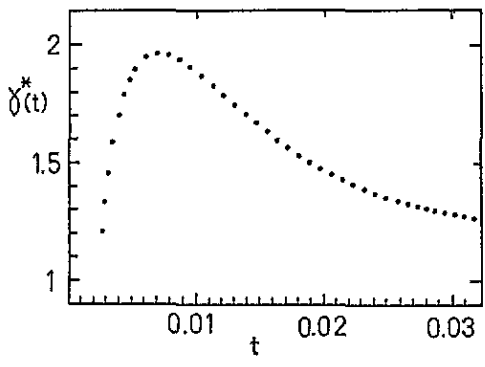

Figure 4. The effective susceptibility exponent $\gamma^*(t)$—defined in equation (5)—plotted against reduced temperature t on a linear scale.

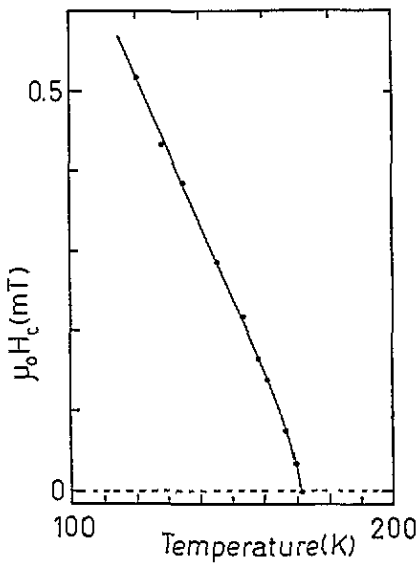

Figure 5. The coercive field $\mu_0 H_c$ (in mT) estimated from butterfly loop measurements, plotted against temperature (in K) in the vicinity of the Curie temperature.

(i) Figure 2 reproduces the fit of (3) to the susceptibility peak data in the form of a double logarithmic plot; this figure confirms this power-law prediction and yields an effective exponent

$$\delta^*(H) = 3.8 \pm 0.2 \qquad 1.5 \leqslant \mu_0 H_a \leqslant 10^2 \text{ mT}.$$

(ii) Figure 3 displays a similar fit of (4) to the (reduced) susceptibility peak temperature, and yields

$$(\gamma^* + \beta^*)^{-1} = 0.57 \pm 0.02 \qquad 1.5 \leqslant \mu_0 H_a \leqslant 10^2 \text{ mT}.$$

(iii) Figure 4 examines the applicability of (2) to the zero-field data, in modified form, by plotting the effective Kouvel–Fisher exponent [17]

$$\gamma^*(T) = \mathrm{d}\ln(\chi(0,t))/\mathrm{d}\ln(t) \tag{5}$$

against t. Two important points emerge from this latter plot: first, the temperature dependence displayed by $\gamma^*(T)$—specifically the maximum near $t = 7 \times 10^{-3}$—is characteristic of a significant variance in the exchange bond distribution between the Fe spins in this random alloy [18–20], and second, the fall in $\gamma^*(T)$ near $t = 3 \times 10^{-3}$ below the localized three-dimensional Heisenberg model value of $\gamma = 1.386$ [21] reflects the failure of $\chi(0,t)$ to reach its demagnetization factor limited value (an *upper* limit on the demagnetization factor N is set by treating the sample as an ellipsoid and evaluating the corresponding elliptic integral [22]; the resulting *lower* limit for the measured susceptibility is then estimated at 1.5×10^4 J T^{-2} kg^{-1}). This last result is usually regarded as a manifestation of anisotropy effects, most likely attributable here to spin–orbit coupling. Direct support for this assignment is also provided by the data in figures 1–3, viz. the inability of applied fields $\mu_0 H_a$ of less than 1.5 mT to resolve a maximum in the field dependent susceptibility above T_C (a critical peak structure becomes evident at fields as low as 4×10^{-2} mT in magnetically soft systems [14]) indicates directly that the technical components in the magnetic response are not driven to saturation in low fields, so the critical component does not dominate the measured susceptibility. Under such conditions *effective* exponent values alone can be quoted, which may *not* represent the true, asymptotic values normally compared through the Widom relation [23]. In the present sample, although the data in figure 4 do not preclude an asymptotic value for γ close to that (1.386) predicted by the localized 3D Heisenberg model [21], and those in figure 3 are consistent with $(\gamma + \beta)$ being equal to the same model prediction of 0.57 [21], the $\delta^*(H)$ value found from figure 2 is 3.8 ± 0.2, well below the corresponding model prediction of 4.8 [21]. However, since these latter data do not extend below 1.5 mT, the asymptotic (low-field) δ value remains uncertain. Indeed, the distribution of exchange coupling strengths inferred from figure 4 would lead to the expectation that $\delta^*(H)$ should increase with decreasing field [14, 24], a prediction that cannot be verified here as the low-field critical peaks remain unresolved for the reasons outlined above.

Nevertheless, these data are consistent with a well defined paramagnetic to ferromagnetic transition occurring in this system (probably with exponents close to localized 3D Heisenberg model values, although the true asymptotic exponent values are difficult to verify due to the presence of anistropy resulting from spin–orbit coupling), at a Curie temperature $T_C = 172.75 \pm 1.5$ K, which was used in constructing figures 3 and 4 (the error in T_C represents uncertainties in the absolute temperature; relative temperatures can be established with a precision approaching 25–50 mK); this estimate for the Curie temperature is in very good agreement with a value of (170 ± 2) K quoted from Mössbauer measurements on a sample of the same nominal composition [25].

3.2. Coercivity

Estimates for the coercive field $\mu_0 H_c$ were obtained from 'butterfly loop' measurements, viz. $\chi_{AC}(H_a, T)$ versus H_a at various fixed temperatures, as previously described [14]. Figure 5 summarizes the temperature dependence of H_c so obtained; this coercive field vanishes at 172 ± 1 K (confirming the estimate for T_C given above), and while the overall magnitude of H_c remains rather small, its rapid increase with decreasing temperature immediately below T_C is consistent with it originating from spin–orbit coupling effects [26].

3.3. Low-temperature magnetoresistivities

Figure 6 shows the field induced change in resistivity

$$\Delta\rho/\rho_0 = [\rho(H_a) - \rho(0)]/\rho(0)$$

measured at 4.2 K in the longitudinal (‖) and transverse (⊥) configurations in applied fields $\mu_0 H_a$ up to 1 T. Due to the large residual resistivity in this system, $\rho(0, 4.2\ \text{K}) \simeq 30.3\ \mu\Omega$ cm (slightly—but not unexpectedly—lower than the extrapolated value of 32 $\mu\Omega$ cm from lower-concentration data [27]), there is very little ordinary magnetoresistance due to cyclotron curvature effects, thus both $\rho_\parallel$ and $\rho_\perp$ are essentially field independent above about 0.25 T. From the data in this figure the spontaneous resistive anisotropy (SRA), defined as [28]

$$\Delta\rho(B \to 0)/\rho_0 = [[\rho_\parallel(B) - \rho_\perp(B)]/\rho_0]_{B\to 0} \tag{6}$$

is estimated as $+(1.44 \pm 0.02)\%$, of the same sign† but larger than that reported at lower concentration (+0.7% [27]). Such an increase in the SRA with increasing concentration is consistent with the behaviour reported in comparable systems [29].

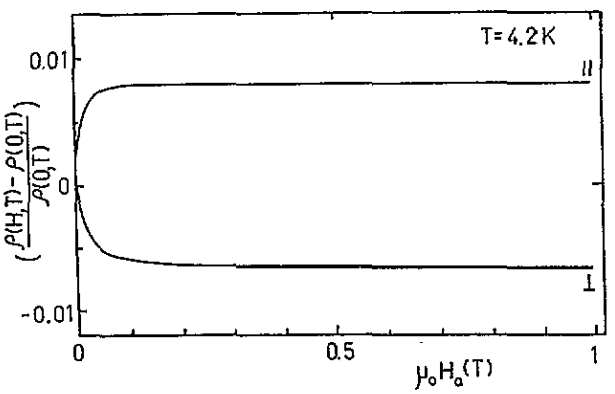

Figure 6. The field induced change in resistivity $[(\rho(H, T) - \rho(0, T))/\rho(0, T)]$ measured at 4.2 K in the longitudinal (‖) and transverse (⊥) configurations. $\rho(0, T = 4.2\ \text{K})$ is estimated at 30.3 $\mu\Omega$ cm (subject to a ±1% uncertainty due to shape factor limitations).

3.4. Zero-field resistivity and its temperature derivative

A summary of the zero-field resistivity, $\rho(0, T)$, measured over the temperature interval 100–200 K using the differential method discussed in section 2, is presented in figure 7. The resistivity values shown in this figure are based on $\rho(0, 110\ \text{K}) = 36.4\ \mu\Omega$ cm, and while this differential technique allows relative resistivity values to be estimated with a precision approaching a few ppm, absolute values are uncertain to typically ±1% due to previously discussed limitations on shape factor measurements.

The temperature derivatives $\mathrm{d}\rho/\mathrm{d}T$, of these zero-field resistivity data are plotted immediately below the $\rho(0, T)$ measurements in figure 7, on the same temperature scale. As with other disordered alloy systems [30], the maximum in this derivative is taken as yielding an estimate for T_C, and figure 7 indicates $T_C = (170 \pm 2.5)$ K with the error here arising from both absolute temperature uncertainties and scatter in the measured

† Here, since the resistivity is essentially independent of the applied field, it is irrelevant whether the extrapolation procedure implicit in (6) is based on H_a or the induction $B(= \mu_0(H_a + M) - DM$, in the usual notation [14]).

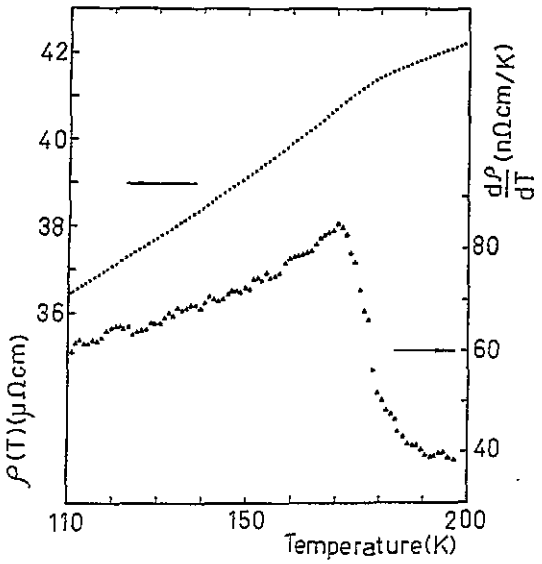

Figure 7. The zero-field resistivity $\rho(0, T)$ (in $\mu\Omega$ cm) and the temperature derivative $d\rho/dT$ (in nΩ cm K^{-1}) plotted against temperature (in K) above and below the ordering temperature.

derivatives. Above 190 K these measured derivatives approach those reported for pure Pt ($d\rho/dT = 39.5$ nΩ cm K^{-1} [31]), and this allows the following estimate to be made for the total spin disorder resistivity $\Delta\rho_M$ in this sample, based upon a Mattheissen's rule type approximation. With $\rho(0, 190\ K) = 41.8\ \mu\Omega$ cm and $\rho(0, 4.2\ K) = 30.3\ \mu\Omega$ cm then $\Delta\rho_M$ is found using

$$\Delta\rho_M = [\rho(0, 190\ K) - \rho(0, 4.2\ K)] - [\rho_{Pt}(190\ K) - \rho_{Pt}(4.2\ K)] = (11.5 - 6.33)\ \mu\Omega\ cm$$
$$= 5.17\ \mu\Omega\ cm. \tag{7}$$

Here $\rho_{Pt}(T)$ represents the resistivity of pure Pt measured at temperature T in zero field (taken from the data of White and Woods [31]). The use of $\rho(0, 190\ K)$ in estimating $\Delta\rho_M$ rather than $\rho(0, T_C)$ allows the effects of short-ranged spin correlations persisting immediately above T_C to be taken into account, i.e. we take the resistivity of the *totally* disordered (paramagnetic) state to be attained at the temperature at which $d\rho/dT$ in the alloy becomes equal to that for the host metal ($T = 190$ K, $t \simeq 10^{-1}$). Furthermore, figure 6 indicates that the spins are not *completely* ordered at 4.2 K, as the average magnetoresistance

$$\rho(H_a, 4.2\ K) = (\rho_{\parallel}(H_a, 4.2\ K) + 2\rho_{\perp}(H_a, 4.2\ K))/3 \tag{8}$$

decreases by approximately 53 nΩ cm between $\mu_0 H_a = 0$ and 1 T. This decrease is consistent with that expected from the field induced suppression of the number of thermally excited spin waves at temperatures well below T_C (i.e. via a field induced gap in the magnon spectrum at $q = 0$ [32]), and its neglect introduces a small error in $\Delta\rho_M$ compared with that from shape factor uncertainties ($\sim \pm 0.1\ \mu\Omega$ cm).

Using a localized s–d model Hamiltonian [33, 34]

$$H_{sd} = V - 2JS \cdot \sigma \tag{9}$$

to describe the scattering of Pt conduction electrons (spin σ) from localized Fe spins (S), in which V represents the screened Coulomb potential due to the deviation of the lattice

potential from perfect periodicity and J is the conduction electron–local moment exchange coupling, enables $\Delta\rho_M$ to be written as [35]

$$\Delta\rho_M = AcJ^2S(1+4S) \tag{10}$$

valid when $V^2 \gg J^2$, and where

$$A = 3\pi m^*\Omega/2\hbar e E_F$$

incorporates details of the band structure (m^* being the s-electron effective mass, Ω the atomic volume and E_F the Fermi energy). Using $A = 9.23\ \mu\Omega$ cm at.%$^{-1}$ eV^{-2} [35] when c is the Fe concentration in atomic percent and V and J are in electron volts (eV), then (7) and (10) yield

$$|J| \simeq 0.04(5)\ \text{eV}$$

(when S is taken as $\frac{5}{2}$ [36]), in good agreement with a value of 0.04(1) eV deduced from magnetoresistance measurements on samples with much lower Fe concentration [36] using the same localized s–d model Hamiltonian [33, 34].

3.5. The low-field resistive anisotropy (LFRA)

Figure 8 reproduces measurements of the LFRA, viz.

$$\Delta\rho(H_a, T)/\rho_0(T) = [\rho_\parallel(H_a, T) - \rho_\perp(H_a, T)]/\rho_0(H_a, T) \tag{11}$$

as a function of temperature T in the vicinity of T_C, in applied fields of $\mu_0 H_a = 2.5$, 6.2, 10 and 12.9 mT. This anisotropy vanishes at the Curie temperature T_C, and the estimate for the latter obtained from these data is (170 ± 1.5) K, again in good agreement with the values deduced from other properties. As discussed previously [10, 11, 37] the occurrence of an anisotropy, whether discussed in terms of itinerant or localized model approaches, relies on two essential factors: (i) a polarizing field; and (ii) an orbital contribution to the moment (with spin–orbit coupling) at the scattering site.

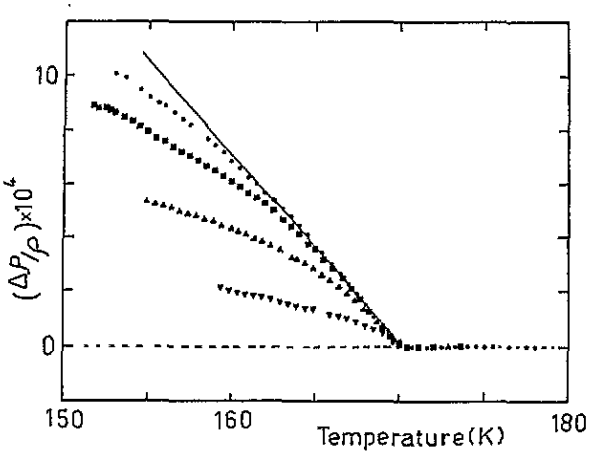

Figure 8. The LFRA $(\rho_\parallel(H_a, T) - \rho_\perp(H_a, T))/\rho_0$ plotted against temperature (in K) above and below the ordering temperature for applied fields $\mu_0 H_a$ (in mT) of 12.9 (●), 10 (■), 6.2 (▲) and 2.5 (▼). The solid line is a guide for the eye and is intended to represent the limiting behaviour for all fields *close* to T_C.

3.5.1. Itinerant models. The application of an itinerant model to alloys such as FePt must account for the Fe induced exchange splitting of the host's band structure. Specifically both transport and magnetic properties acquire separate contributions from spin up (+) and spin down (−) sub-bands, resulting from a difference in the behaviour of electrons near the Fermi energy depending on their spin orientation. The total resistivity $\rho(T)$ thus reflects contributions from these sub-bands ($\rho_+(T)$ and $\rho_-(T)$) acting in parallel, with spin flip scattering ($\rho_\pm(T)$) effecting a transfer of electrons between the two spin labelled sub-bands; this yields [11, 38]

$$\rho(T) = [\rho_+(T)\rho_-(T) + \rho_\pm(T)\{\rho_+(T) + \rho_-(T)\}]/[\rho_+(T) + \rho_-(T) + 4\rho_\pm(T)] \ldots . \quad (12)$$

A frequently assumed form for spin flip resistivity is [39]

$$\rho_\pm(T) = DT^2 \quad (13)$$

although if this process arises from electron–magnon scattering this form overestimates the spin flip contribution at higher temperatures [40], as might be anticipated (as single-particle excitations replace collective modes, particularly near T_C). As mentioned above, the occurrence of an anisotropy in the magnetoresistance relies on the presence of a spin–orbit interaction ($\lambda \boldsymbol{L} \cdot \boldsymbol{S}$ in the usual notation), the off diagonal elements of which couple various orbitally labelled states in *different* spin sub-bands. The latter are split by the presence of the exchange field (H_{ex}), although *within* each sub-band the $(2\ell + 1)$ orbital subgroups are treated as degenerate. While such admixture is relatively straightforward to treat in, say, a tight-binding d band approach, a useable expression describing the magnetoresistive anisotropy requires a variety of further assumptions to be made. Malozemoff [41, 42] has modified and extended such an approach to situations where there is a substantial spin up and spin down d band density of states at the Fermi energy, and where each sub-band resistivity contains both s → s and s → d scattering contributions (so that $\rho_+ = \rho_{ss+} + \rho_{sd+}$, etc). This latter approach, when spin flip contributions—although assumed to be unaffected by spin–orbit coupling—are nevertheless retained, and remembering that the spin–orbit mediated anisotropy, by definition, can only originate from processes involving the d bands (more correctly, processes outside the s bands), yields

$$\Delta\rho/\rho \simeq \gamma[\rho_- - \rho_+][\rho_{sd-} - \rho_{sd+}]/[\rho_+\rho_- + \rho_\pm(\rho_+ + \rho_-)]. \quad (14)$$

Here γ, proportional to $\lambda^2(K^2 \pm H_{ex}^2)^{-1}$, incorporates the effects of a cubic anisotropy (K) term [41], a necessity if the 'catastrophe' resulting from the divergence in γ as the exchange field collapses at T_C is to be avoided. A further, reasonable approximation in alloys such as $Fe_{10}Pt_{90}$ would be to take

$$\rho_{ss+} \simeq \rho_{ss-}$$

(the exchange splitting, as with the induced (giant) moment, is confined predominantly to the d bands), then

$$\Delta\rho/\rho \simeq \gamma[\rho_{sd-} - \rho_{sd+}]^2/[\rho_+\rho_- + \rho_\pm(\rho_+ + \rho_-)]. \quad (15)$$

For comparison with experiment, further assumptions have to be made, particularly regarding the numerator in (15); close to T_C, an expansion of ρ_{sd} in terms of the exchange field H_{ex} leads to [42]

$$\rho_{sd+,-} \simeq \rho_{sd}(0) \pm sH_{ex} \ldots \quad (16)$$

where s, the derivative of the d sub-band resistivity with respect to the exchange field, would be determined primarily by the slope of the corresponding density of states near the Fermi energy E_F, so

$$\frac{\Delta\rho}{\rho} \simeq \frac{(\lambda/K)^2(dN/dE)^2_{E_F}H^2_{ex}}{\rho_+\rho_- + \rho_\pm(\rho_+ + \rho_-)}. \tag{17}$$

In mean field, H_{ex} becomes proportional to the thermal average of the spontaneous magnetization, $\langle M\rangle_T$, the temperature dependence of which, in standard collective electron/band theory is given by [43]

$$\langle M\rangle_T \propto (T - T_C)^{1/2}.$$

Combining all of these approximations yields

$$\frac{\Delta\rho}{\rho} \propto \frac{(\lambda/K)^2(dN/dE)^2_{E_F}(T - T_C)}{\rho_+\rho_- + \rho_\pm(\rho_+ + \rho_-)} \tag{18}$$

a result that indicates that the anisotropy increases linearly with decreasing temperature below T_C, *provided the other terms in (18)—particularly the spin-flip resistivity* $\rho_\pm$*—are relatively insensitive to temperature in this region*; this prediction is consistent with the behaviour of the measured LFRA, as discussed below. The above arguments are clearly quite qualitative, and a more careful comparison with itinerant model results would necessitate a detailed calculation of the numerous contributions in (18), involving realistic band structure effects, k dependent matrix elements, spin flip scattering near T_C, etc. Despite recent advances in such calculations, particularly using LSDA techniques [44] for example, they are currently unable to yield such detailed information, thus precluding a quantitative appraisal of the influence of such factors as compositional changes. The above arguments, despite their qualitative nature, clearly do not indicate the inadmissibility of such models.

3.5.2. Localized models. Despite some intuitive objections to their use, localized models also predict a temperature dependence for the anisotropy, consistent with experimental observation. Here the spin dipole moment (S) is aligned by the polarizing field which, through spin–orbit coupling, results in a preferential orientation of any orbital (L) component. For $L \neq 0$, the associated non-spherical charge distribution leads to a slightly different scattering cross-section for the conduction electrons constituting the current as the relative alignment of the current and the field are changed. In the present experiment the *exchange* field (which collapses at T_C) is the polarizing agent; the (small) applied field serves simply to define a quantization axis for spin–orbit coupling (essentially by rendering the system single domain over length scales comparable to a conduction electron mean free path). A detailed analysis within such an approach is obtained by carrying out a multipole moment expansion of the non-spherical *charge* distribution, and this reveals that to lowest order the asymmetry results from *electric quadrupole* scattering effects (*electric* dipole terms vanish in a central field), so that the associated Hamiltonian $\mathcal{H}$ for conduction electron scattering becomes [11]

$$\mathcal{H} = \sum_{k,k'}\left[V + JS\cdot\sigma - \frac{D}{k_F^2}\{(S\cdot k)(S\cdot k') - S(S+1)k\cdot k'/3\}\right]a^\dagger_{k'}a_k \ldots. \tag{19}$$

Here V is the screened Coulomb potential, $JS\cdot\sigma$ the *magnetic dipole* or exchange coupling between a localized spin (S) and a conduction electron (spin σ), with the last

term representing scattering from the electric quadrupole moment (D). In single crystals, both of the first two terms can be anisotropic [45], but in polycrystalline or amorphous environments any asymmetry in the magnetoresistance arises from the final term (which is referenced to the field direction rather than any crystallographic direction); in the often realized limit $V^2 \gg J^2$, D^2 this asymmetry can be written as

$$[\rho_{\parallel}(B) - \rho_{\perp}(B)]/\rho_0 \simeq (D/V)[\langle S_Z^2 \rangle - S(S+1)/3]. \tag{20}$$

We have calculated these quadrupolar asymmetries using a localized model based on an effective field Ising Hamiltonian [46, 47] incorporating a uniform applied field and a Gaussian distribution of exchange coupling strengths between localized spins. In this latter model the thermal average implicit in (20) is replaced by the double average $\langle\langle S_Z^2 \rangle_T \rangle_J$ (where $\langle\rangle_T$ represents a thermal and $\langle\rangle_J$ an exchange average), and the LFRA is predicted to behave as

$$\Delta\rho/\rho_0 = A(\eta)[(T - T_C)/T_C] \qquad T < T_C. \tag{21}$$

Localized models thus indicate the same linear increase of the anisotropy with decreasing temperature below T_C as do itinerant models, although with less restrictive assumptions. Furthermore, the anisotropy *ratio* appearing in (21) is essentially independent of band structure details (which contribute in a comparable manner to both numerator and denominator) in contrast to itinerant model expressions (18), and this enables the influence of other variables to be assessed rather directly. Specifically, localized models predict that the coefficient $A(\eta)$ should increase with decreasing bond disorder (in the particular model adopted here this means an increase in the ratio $\eta = \bar{J}_0/\bar{J}$ of the first to second moment of (assumed) Gaussian exchange bond distribution), a conclusion that would be far more difficult to arrive at from itinerant models at current levels of understanding. While the influence of the exchange distribution is not being investigated here, recently reported results on both the measured temperature dependence of the LFRA immediately below T_C in FeZr metallic glasses and the behaviour of $A(\eta)$ with hydrogen loading (the dilation associated with the introduction of hydrogen modifies the exchange bond distribution) provide a further favourable comparison with (21) [10]. A further comparison that is made here, however, is between the data reproduced in figure 8 and the localized model prediction summarized in figure 9 for the *applied* field dependence of the quadrupolar operator $[\langle\langle S_Z^2 \rangle_T \rangle_J - S(S+1)/3]$ near T_C (for a fixed exchange bond distribution corresponding to $\eta = 2.5$). The quantitative calculations contained in this latter figure indicate that the LFRA should be independent of H_a (over the field range covered by the data in figure 8) near T_C, a result that also appears consistent with qualitative arguments based on itinerant models, provided that the density of states is reasonably smooth. These model approaches however do *not* include domain effects, and while the data in figure 8 do approach a field independent limiting slope very close to T_C (in agreement with the corresponding model predictions), the progressive deviations from predicted behaviour below T_C with decreasing applied field are, we suggest, due to the failure of low fields to maintain the constraint mentioned above, viz. that these fields render the system single domain over length scales comparable to the electronic mean free path.

4. Summary and conclusion

The results of detailed measurements in $Fe_{10}Pt_{90}$ of the longitudinal and transverse magnetoresistivities and the AC magnetic susceptibility have been presented. In the case

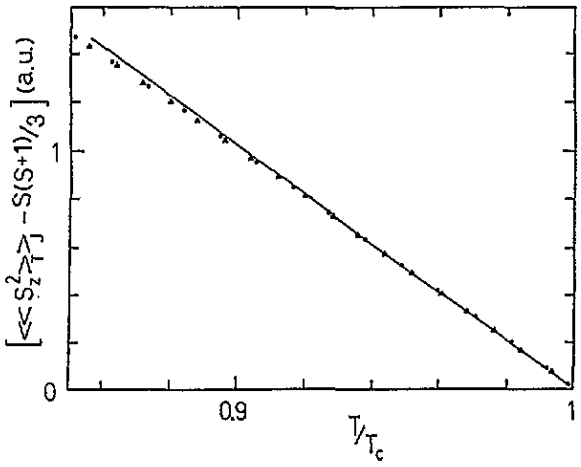

Figure 9. The calculated quadrupolar term $\langle(S_Z^2)_T\rangle_J - S(S+1)/3$ (in arbitrary units) plotted against reduced temperature T/T_C; for $T_C = 170$ K these calculations correspond to $\mu_0 H_a$ (in mT) of 11.7 (●) and 2.9 (▲). The solid line represents equation (21).

of the latter, these data have been analysed to yield estimates for 'effective' exponents as the true asymptotic exponent values appear obscured by effects originating in spin–orbit coupling, a coupling also necessary for the observation of a resistive anisotropy. Estimates for the Curie temperature obtained from these different measurements are also compared. Apart from providing insight into the fundamental magnetic properties of this system, these data also supply a useful background against which spin–orbit coupling effects can be assessed; as far as the magnetic properties are concerned, such a coupling certainly obscures the emerging critical peaks (as discussed in section 3.1) but to no greater extent than in, say, AuFe of comparable composition [48]. Since GMR effects are observed in granular samples of this latter system, this would suggest that the spin–orbit interaction is *not* the dominant cause of the failure to observe such anomalies in FePt, in agreement with very recent studies [49] of the microstructure of this system which conclude that its failure to exhibit GMR results from it being a homogeneous solid solution not a heterogeneous granular material.

References

[1] Baibich M N, Broto J M, Fert A, Nguyen Van Dau F, Petroff F, Eitenne P, Creuzet G, Friederich A and Chazelas J 1988 *Phys. Rev. Lett.* **61** 2472

[2] Camley R E and Barnas J 1989 *Phys. Rev. Lett.* **63** 664

[3] Parkin S S P, More N and Roche K P 1990 *Phys. Rev. Lett.* **64** 2304

[4] Levy P M, Zhang S and Fert A 1990 *Phys. Rev. Lett.* **65** 1643

[5] Xiao J Q, Jiang J S and Chien C L 1992 *Phys. Rev. Lett.* **68** 3749

[6] Berkowitz A E, Mitchell J R, Carey M J, Young A P, Zhang S, Spada F E, Parker F T, Hutten A and Thomas G 1992 *Phys. Rev. Lett.* **68** 3745

[7] Wang J Q, Xiong P and Xiao G 1993 *Phys. Rev.* B **47** 8341

[8] 1994 *Proc. 38th Annual Conf. on Magnetism and Magnetic Materials (Minneapolis, 1993); J. Appl. Phys.*

[9] Wang J Q, Xiong P and Xiao G 1994 *J. Appl. Phys.* at press

[10] Stampe P A, Kunkel H P and Williams G 1993 *J. Phys : Condens. Matter* **5** L625

[11] Friederich A and Fert A 1974 *Phys. Rev. Lett.* **33** 1214
Fert A, Asomoza R, Sanchez D H, Spanjaard D and Friederich A 1977 *Phys. Rev.* B **16** 5040
Campbell I A and Fert A 1982 *Ferromagnetic Materials* vol 3, ed E P Wohlfarth (Amsterdam: North-Holland) p 747

[12] Ododo J C 1979 *J. Phys. F: Met. Phys.* **9** 1441

[13] Maartense I 1970 *Rev. Sci. Instrum.* **41** 657

[14] Williams G 1991 *Magnetic Susceptibility of Superconductors and Other Spin Systems* ed R A Hein *et al* (New York: Plenum) p 475
Wang Z, Kunkel H P and Williams G 1992 *J. Phys.: Condens. Matter* **4** 10385
[15] Muir W B and Ström-Olsen J O 1976 *J. Phys. E: Sci. Instrum.* **9** 163
[16] Stanley H E 1971 *Introduction to Phase Transitions and Critical Phenomena* (Oxford: Clarendon)
[17] Kouvel J S and Fisher M E 1964 *Phys. Rev.* A **136** 1626
[18] Gaunt P, Ho S C, Williams G and Cochrane R W 1981 *Phys. Rev.* B **23** 251
[19] Kaul S N 1985 *J. Magn. Magn. Mater.* **53** 5
[20] Holey T and Fähnle M 1987 *Phys. Status Solidi* b **141** 253
[21] LeGuillou L C and Zinn-Justin J 1980 *Phys. Rev.* B **21** 3976
[22] Osborn J A 1945 *Phys. Rev.* **67** 351
[23] Widom B 1965 *J. Chem. Phys.* **43** 3898
[24] Roshko R M and Williams G 1984 *J. Phys. F: Met. Phys.* **14** 703
Kornik K, Kunkel H P, Roshko R M and Williams G 1990 *Solid State Commun.* **76** 993
[25] Segnan R 1967 *Phys. Rev.* **160** 404
[26] Morrish A H 1980 *Physical Principles of Magnetism* (New York: Krieger)
[27] Hamzić A 1980 *Thesis* Université de Paris-Sud
[28] Dorleijn J W F 1976 *Philips Res. Rep.* **31** 287
[29] Senoussi S, Campbell I A and Fert A 1977 *Solid State Commun.* **21** 269
[30] Mydosh J A, Budnick J I, Kawatra M P and Skalski S 1968 *Phys. Rev. Lett.* **21** 1346
Kawatra M P, Budnick J I and Mydosh J A 1970 *Phys. Rev.* B **2** 1587
[31] White G K and Woods S B 1959 *Phil. Trans. R. Soc.* A **251** 273
[32] Hamzić A and Campbell I A 1978 *J. Phys. F: Met. Phys.* **8** L33
[33] Kasuya T 1956 *Prog. Theor. Phys.* **16** 45
[34] Yosida K 1957 *Phys. Rev.* **106** 893
[35] Bews J, Sheikh A W and Williams G 1986 *J. Phys. F: Met. Phys* **16** 1537
[36] Swallow G A, Williams G, Grassie A D C and Loram J W 1971 *J. Phys. F: Met. Phys.* **1** 511
[37] Ma H, Wang Z, Kunkel H P and Williams G 1992 *J. Phys.: Condens. Matter* **4** 1993
Kunkel H P, Wang Z and Williams G 1989 *J. Phys.: Condens. Matter* **1** 3381, 1987 *J. Phys. F: Met. Phys.* **17** L157
[38] Campbell I A, Fert A and Jaoul O 1970 *J. Phys. C: Solid State Phys.* **3** S95
[39] Fert A and Campbell I A 1968 *Phys. Rev. Lett.* **21** 1190
[40] Fert A 1969 *J. Phys. C: Solid State Phys.* **2** 1784
[41] Malozemoff A P 1985 *Phys. Rev.* B **32** 6080
[42] Malozemoff A P 1986 *Phys. Rev.* B **34** 1853
[43] Wilson A H 1965 *The Theory of Metals* (Cambridge: Cambridge University Press)
[44] Brooks M S S, Eriksson O, Johansson B, Franse J M M and Frings P H 1988 *J. Phys. F: Met. Phys.* **18** L33
Metz A, Frota-Pessôa S, Kapoor J and Riegel D 1993 *Phys. Rev. Lett.* **71** 3525
Eriksson O, Brooks M S S and Johansson B 1990 *Phys. Rev.* B **47** 7311
[45] Press M J and Hedgcock F T 1969 *Phys. Rev. Lett.* **23** 167
[46] Kaneyoshi T 1975 *J. Phys. C: Solid State Phys.* **8** 3415
[47] Southern B W 1976 *J. Phys. C: Solid State Phys.* **9** 4011
[48] Maartense I and Williams G 1978 *Phys. Rev.* B **23** 251
[49] Wang J Q and Xiao G 1994 *Phys. Rev.* B **49** 3982